PERGAMON

International Journal of Solids and Structures 38 (2001) 1265–1280

INTERNATIONAL JOURNAL OF SOLIDS and STRUCTURES

www.elsevier.com/locate/ijsolstr

The dynamic stress intensity factor for a semi-infinite crack in orthotropic materials with concentrated shear impact loads

C.Y. Wang, C. Rubio-Gonzalez, J.J. Mason *

Department of Aerospace and Mechanical Engineering, University of Notre Dame, 378 Fitzpatrick Hall, Notre Dame, IN 46556-5637, USA

Received 15 October 1998; in revised form 2 March 2000

Abstract

The transient elastodynamic response of an orthotropic material due to concentrated shear impact loads on the faces of a semi-infinite crack is examined, and the solution for the stress intensity factor history around the crack tip is found. Laplace and Fourier transforms together along with the Wiener–Hopf technique are employed to solve the equations of motion. Even though the problem has characteristic length, it has been shown in previous works that the Wiener–Hopf technique can be applied. The asymptotic expression of stress near the crack tip is analyzed, which leads to the dynamic mode II stress intensity factor. The results are presented for orthotropic materials as well as for an isotropic material. © 2001 Elsevier Science Ltd. All rights reserved.

Keywords: Shear impact loads; Orthotropic materials; Stress intensity factor

1. Introduction

The increasing use of composites in many engineering applications demands a fundamental understanding of the response of cracked orthotropic bodies to impact loading. By using the integral transform methods, the dynamic behavior for a finite crack under concentrated loads (Rubio-Gonzalez and Mason, 1998a,b) as well as for a semi-infinite crack under concentrated or uniform normal loads (Rubio-Gonzalez and Mason, 1998c,d) on its faces in orthotropic materials have been analyzed by Rubio-Gonzalez and Mason. In the former, the finite crack problem is reduced to a Fredholm integral equation in the Laplace transform domain which is solved numerically, and in the latter for the Wiener–Hopf technique was used to find the stress ahead of the crack tip and the displacement on the crack faces. The asymptotic expression for the stress near the crack tip leads to the stress intensity factor $K(t)$.

Many solutions for various loadings of cracks in orthotropic materials have been found by applying transforms to the displacement formulation of the equations of motion. Where previous researchers (Kassir and Bandyopadhyay, 1983) following this approach had solved the resulting dual integral equations using

* Corresponding author. Tel.: +1-219-631-9370; fax: +1-219-631-8341.
E-mail address: mason.12@nd.edu (J.J. Mason).

0020-7683/01/$ - see front matter
PII: S0020-7683(00)00056-1

the method of Sneddon (1946, 1952), Rubio-Gonzalez and Mason (1998c) solved the same equations by converting the dual integral equations to a Wiener–Hopf equation. Solution of that equation requires only a straight forward application of the method of Noble 1958. In this paper, the problem of concentrated shear impact loads on the faces of a semi-infinite crack in orthotropic materials is analyzed using the same method. While it has been thought that the Wiener–Hopf technique could not be applied to problems such as this (Freund, 1974, 1990), this approach has recently been shown to be valid in such cases (Kuo and Chen, 1992). By combining Laplace and Fourier transforms with the Wiener–Hopf technique, a solution for the stress ahead of the crack tip is sought. The asymptotic expression for the stress near the crack tip leads to the mode II stress intensity factor, $K_{II}(t)$.

2. Description of the problem

The plane problem of an infinite orthotropic body containing a semi-infinite crack is considered in Fig. 1. Let E_i, μ_{ij} and v_{ij} $(i,j=1,2,3)$ be the engineering elastic constants of the material wherein the indices (1, 2 and 3), respectively, stand for the directions (x, y, z) of a Cartesian coordinate system chosen to coincide with the orthotropic axes of a material. The crack faces are suddenly loaded by a pair of concentrated shear forces with a magnitude (q) located at a distance (a) away from the crack tip, as shown in Fig. 1.

2.1. Equations of motion

The following problem is limited to a two-dimensional case with the inertial effect in the x–y plane only. By setting all the derivatives with respect to z-direction to be zero, it is readily shown that the displacement equations of motion (Nayfeh, 1995) reduce to

$$\begin{aligned} c_{11}\frac{\partial^2 u}{\partial x^2}+\frac{\partial^2 u}{\partial y^2}+(1+c_{12})\frac{\partial^2 v}{\partial x\,\partial y}&=\frac{1}{c_s^2}\frac{\partial^2 u}{\partial t^2},\\ \frac{\partial^2 v}{\partial x^2}+c_{22}\frac{\partial^2 v}{\partial y^2}+(1+c_{12})\frac{\partial^2 u}{\partial x\,\partial y}&=\frac{1}{c_s^2}\frac{\partial^2 v}{\partial t^2}, \end{aligned} \tag{1}$$

where u and v are the x and y components of the displacement vector, respectively. In the orthotropic solids, $c_s=\sqrt{\mu_{12}/\rho}$ represents the velocity of the shear wave propagating along the principle material axes on the xy-plane and ρ is the mass density. Here also, we introduce the velocity $c_d=\sqrt{c_{11}}c_s$, which will appear later, representing the dilational wave speed along the x-axis. The non-dimensional parameters c_{11}, c_{12} and c_{22} are related to the elastic constants by the following relations. For a generalized plane stress problem,

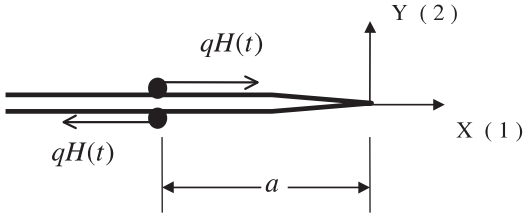

Fig. 1. Schematic of the semi-infinite crack under concentrated shear impact loads.

$$
\begin{aligned}
c_{11} &= \frac{E_1}{\mu_{12}[1-(E_2/E_1)v_{12}^2]},\\
c_{22} &= (E_2/E_1)c_{11},\\
c_{12} &= v_{12}c_{22} = v_{21}c_{11}.
\end{aligned}
\tag{2}
$$

For a plane strain problem,

$$
\begin{aligned}
c_{11} &= \frac{E_1}{\mu_{12}\Delta}(1-v_{23}v_{32}),\\
c_{22} &= \frac{E_2}{\mu_{12}\Delta}(1-v_{13}v_{31}),\\
c_{12} &= \frac{E_1}{\mu_{12}\Delta}\left(v_{21}+\frac{E_2}{E_1}v_{13}v_{32}\right),\\
\Delta &= 1-v_{12}v_{21}-v_{23}v_{32}-v_{31}v_{13}-v_{12}v_{23}v_{31}-v_{13}v_{21}v_{32},\\
\frac{v_{ji}}{E_j} &= \frac{v_{ij}}{E_i} \quad (i,j=1,2,3).
\end{aligned}
\tag{3}
$$

Finally, the stresses are related to the displacements by the equations,

$$
\begin{aligned}
\frac{\sigma_x}{\mu_{12}} &= c_{11}\frac{\partial u}{\partial x}+c_{12}\frac{\partial v}{\partial y},\\
\frac{\sigma_y}{\mu_{12}} &= c_{12}\frac{\partial u}{\partial x}+c_{22}\frac{\partial v}{\partial y},\\
\frac{\tau_{xy}}{\mu_{12}} &= \frac{\partial u}{\partial y}+\frac{\partial v}{\partial x}.
\end{aligned}
\tag{4}
$$

2.2. Boundary conditions and initial conditions

For the case shown in Fig. 1, the pair of spatially concentrated shear loads is applied suddenly on the crack faces. Exploiting symmetry and limiting ourselves to the upper half-plane, $y > 0$, the corresponding boundary conditions become

$$
\begin{aligned}
&\sigma_y(x,0,t) = 0, \quad -\infty < x < +\infty,\\
&\tau_{xy}(x,0,t) = -qH(t)\,\delta(x+a), \quad -\infty < x < 0,\\
&u(x,0,t) = 0, \quad 0 < x < +\infty,
\end{aligned}
\tag{5}
$$

where q is the force per unit length in the z-direction of the opposed line loads acting on the crack faces and $H(t)$ is the unit step function. The Dirac delta function, $\delta(x+a)$, has the dimension of length^{-1}. In addition, the displacement at infinity is zero, and the body is stress-free and at rest everywhere for $t \leqslant 0$.

3. Integral transforms

3.1. Laplace transform

In Eq. (1), the time variable may be replaced by the application of Laplace transform

$$f^*(s) = \int_0^\infty f(t)\mathrm{e}^{-st}\,\mathrm{d}t, \qquad f(t) = \frac{1}{2\pi\mathrm{i}}\int_{\mathrm{Br}} f^*(s)\mathrm{e}^{st}\,\mathrm{d}s = \frac{1}{2\pi\mathrm{i}}\int_{\sigma-i\infty}^{\sigma+i\infty} f^*(s)\mathrm{e}^{st}\,\mathrm{d}s, \tag{6}$$

where Br denotes the Bromwich path of integration, which is a line parallel to the imaginary axis in the s-plane. Thus, using the Laplace transform representation, the displacements have the form,

$$\begin{aligned} u(x,y,t) &= \frac{1}{2\pi\mathrm{i}}\int_{\mathrm{Br}} u^*(x,y,s)\mathrm{e}^{st}\,\mathrm{d}s, \\ v(x,y,t) &= \frac{1}{2\pi\mathrm{i}}\int_{\mathrm{Br}} v^*(x,y,s)\mathrm{e}^{st}\,\mathrm{d}s. \end{aligned} \tag{7}$$

Applying the relations (7) to Eq. (1) and assuming zero initial condition, the transformed domain equations become

$$\begin{aligned} &c_{11}\frac{\partial^2 u^*}{\partial x^2} + \frac{\partial^2 u^*}{\partial y^2} + (1+c_{12})\frac{\partial^2 v^*}{\partial x\,\partial y} - \frac{s^2}{c_s^2}u^* = 0, \\ &\frac{\partial^2 v^*}{\partial x^2} + c_{22}\frac{\partial^2 v^*}{\partial y^2} + (1+c_{12})\frac{\partial^2 u^*}{\partial x\,\partial y} - \frac{s^2}{c_s^2}v^* = 0. \end{aligned} \tag{8}$$

Applying the relation (7) to Eq. (4), the transformed domain relations between stresses and displacements become

$$\begin{aligned} \frac{\sigma_x^*}{\mu_{12}} &= c_{11}\frac{\partial u^*}{\partial x} + c_{12}\frac{\partial v^*}{\partial y}, \\ \frac{\sigma_y^*}{\mu_{12}} &= c_{12}\frac{\partial u^*}{\partial x} + c_{22}\frac{\partial v^*}{\partial y}, \\ \frac{\tau_{xy}^*}{\mu_{12}} &= \frac{\partial u^*}{\partial y} + \frac{\partial v^*}{\partial x}. \end{aligned} \tag{9}$$

Finally, the application of the Laplace transform to the boundary conditions (5) gives

$$\begin{aligned} &\sigma_y^*(x,0,s) = 0, \quad -\infty < x < +\infty, \\ &\tau_{xy}^*(x,0,s) = -q/s\,\delta(x+a), \quad -\infty < x < 0, \\ &u^*(x,0,s) = 0, \quad 0 < x < +\infty. \end{aligned} \tag{10}$$

3.2. Fourier transform

To obtain a solution for differential Eq. (8) subject to condition (10), the Fourier transform is applied,

$$\tilde{f}(\omega) = \int_{-\infty}^{\infty} f(x)\mathrm{e}^{\mathrm{i}\omega x}\,\mathrm{d}x, \qquad f(x) = \frac{1}{2\pi}\int_{-\infty}^{\infty}\tilde{f}(\omega)\mathrm{e}^{-\mathrm{i}\omega x}\,\mathrm{d}\omega. \tag{11}$$

It is noted that the boundary conditions (10) are explicitly defined only on half of the range of x. Consequently, the Fourier transform cannot be applied to these boundary conditions. To remedy this situation, the boundary conditions must be extended to apply on the full range of x. Two-unknown functions $u_-^*(x,s)$ and $\tau_+^*(x,s)$ are introduced. The function $u_-^*(x,s)$ is defined to be the x-direction displacement of the crack face, $y=0$, for $-\infty < x < 0$ and $0 < t < +\infty$, and to be identically zero for $0 < x < +\infty$ and $0 < t < +\infty$. Likewise, the function $\tau_+^*(x,s)$ is defined to be the shear stress in the x-direction on the plane, $y=0$, for $0 < x < +\infty$ and $0 < t < +\infty$, and to be identically zero for $-\infty < x < 0$ and $0 < t < +\infty$. With these definitions, the boundary conditions (10) can be rewritten as

$$\begin{aligned}
&\sigma_y^*(x,0,s) = 0, \quad \text{for } -\infty < x < +\infty,\\
&\tau_{xy}^*(x,0,s) = -q/s\,\delta(x+a) + \tau_+^*(x,s), \quad \text{for } -\infty < x < +\infty,\\
&u^*(x,0,s) = u_-^*(x,s), \quad \text{for } -\infty < x < +\infty.
\end{aligned} \tag{12}$$

Thus, the Laplace transformed displacements have the form

$$\begin{aligned}
u^*(x,y,s) &= \frac{1}{2\pi}\int_{-\infty}^{\infty} \tilde{u}^*(\omega,y,s)\mathrm{e}^{-\mathrm{i}\omega x}\,\mathrm{d}\omega,\\
v^*(x,y,s) &= \frac{1}{2\pi}\int_{-\infty}^{\infty} \tilde{v}^*(\omega,y,s)\mathrm{e}^{-\mathrm{i}\omega x}\,\mathrm{d}\omega.
\end{aligned} \tag{13}$$

Substituting these transforms into Eq. (8), the functions $\tilde{u}^*$ and $\tilde{v}^*$ are found to satisfy the ordinary differential equations

$$\frac{\mathrm{d}^2\tilde{u}^*}{\mathrm{d}y^2} - (1+c_{22})\omega\mathrm{i}\frac{\mathrm{d}\tilde{v}^*}{\mathrm{d}y} - \left(c_{11}\omega^2 + \frac{s^2}{c_\mathrm{s}^2}\right)\tilde{u}^* = 0, \quad c_{22}\frac{\mathrm{d}^2\tilde{v}^*}{\mathrm{d}y^2} - (1+c_{12})\omega\mathrm{i}\frac{\mathrm{d}\tilde{u}^*}{\mathrm{d}y} - \left(\omega^2 + \frac{s^2}{c_\mathrm{s}^2}\right)\tilde{v}^* = 0. \tag{14}$$

The solution of Eq. (14) under the condition of zero displacement at infinity is

$$\begin{aligned}
\tilde{u}^*(\omega,y,s) &= A_1(\omega,s)\mathrm{e}^{-\gamma_1 y} + A_2(\omega,s)\mathrm{e}^{-\gamma_2 y},\\
\tilde{v}^*(\omega,y,s) &= -\frac{\mathrm{i}\alpha_1}{\omega}A_1(\omega,s)\mathrm{e}^{-\gamma_1 y} - \frac{\mathrm{i}\alpha_2}{\omega}A_2(\omega,s)\mathrm{e}^{-\gamma_2 y},
\end{aligned} \tag{15}$$

where $A_1(\omega,s)$ and $A_2(\omega,s)$ are arbitrary functions, and $\alpha_i(\omega,s)$ stands for the functions

$$\alpha_i(\omega,s) = \frac{c_{11}\omega^2 + s^2/c_\mathrm{s}^2 - \gamma_i^2}{(1+c_{12})\gamma_i} \quad (i=1,2) \tag{16}$$

with γ_1^2 and γ_2^2 being two roots of the quadratic equation,

$$c_{22}\gamma^4 + [(c_{12}^2 + 2c_{12} - c_{11}c_{22})\omega^2 - (1+c_{22})s^2/c_\mathrm{s}^2]\gamma^2 + (c_{11}\omega^2 + s^2/c_\mathrm{s}^2)(\omega^2 + s^2/c_\mathrm{s}^2) = 0. \tag{17}$$

The branches of γ_1 and γ_2 are chosen in the appropriate Riemann sheets, and they are real and positive. It has been shown by Willis (1973) and Poruchikov (1993) that such a restriction on γ_1 and γ_2 is possible for the general anisotropic case as long as $\mathrm{Re}\{\omega\} > 0$. This fact is a consequence of the positive definiteness of the strain energy. From Eq. (17), it is readily found that the functions $\gamma_1(\omega)$ and $\gamma_2(\omega)$ are multiple valued at $\omega = \pm\mathrm{i}s/c_\mathrm{s}$ and $\omega = \pm\mathrm{i}s/c_\mathrm{d}$. Such points are called as branch points. That means, the functions γ_1 and γ_2 are analytic everywhere in the complex plane except at the branch points $\omega = \pm\mathrm{i}s/c_\mathrm{s}$ and $\omega = \pm\mathrm{i}s/c_\mathrm{d}$, and are single valued in the ω-plane provided the branch cuts between $\omega = \pm\mathrm{i}s/c_\mathrm{s}$ and $\omega = \pm\mathrm{i}s/c_\mathrm{d}$ shown in Fig. 2 (Freund, 1990).

Thus, the expressions for the displacements in the Laplace transform domain become

$$\begin{aligned}
u^* &= \frac{1}{2\pi}\int_{-\infty}^{\infty}(A_1\mathrm{e}^{-\gamma_1 y} + A_2\mathrm{e}^{-\gamma_2 y})\mathrm{e}^{-\mathrm{i}\omega x}\,\mathrm{d}\omega,\\
v^* &= \frac{-\mathrm{i}}{2\pi}\int_{-\infty}^{\infty}(\alpha_1 A_1\mathrm{e}^{-\gamma_1 y} + \alpha_2 A_2\mathrm{e}^{-\gamma_2 y})\frac{\mathrm{e}^{-\mathrm{i}\omega x}}{\omega}\,\mathrm{d}\omega.
\end{aligned} \tag{18}$$

Substituting these displacements into the constitutive law (9), we obtain

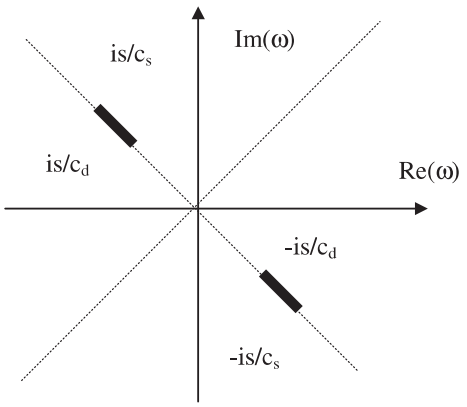

Fig. 2. Branch cuts in the ω-plane.

$$\begin{aligned}
\frac{\sigma_x^*}{\mu_{12}} &= -\frac{\mathrm{i}c_{11}\omega}{2\pi}\int_{-\infty}^{\infty}(A_1\mathrm{e}^{-\gamma_1 y}+A_2\mathrm{e}^{-\gamma_2 y})\mathrm{e}^{-\mathrm{i}\omega x}\,\mathrm{d}\omega+\frac{\mathrm{i}c_{12}}{2\pi}\int_{-\infty}^{\infty}(\alpha_1\gamma_1 A_1\mathrm{e}^{-\gamma_1 y}+\alpha_2\gamma_2 A_2\mathrm{e}^{-\gamma_2 y})\frac{\mathrm{e}^{-\mathrm{i}\omega x}}{\omega}\,\mathrm{d}\omega,\\
\frac{\sigma_y^*}{\mu_{12}} &= -\frac{\mathrm{i}c_{12}\omega}{2\pi}\int_{-\infty}^{\infty}(A_1\mathrm{e}^{-\gamma_1 y}+A_2\mathrm{e}^{-\gamma_2 y})\mathrm{e}^{-\mathrm{i}\omega x}\,\mathrm{d}\omega+\frac{\mathrm{i}c_{22}}{2\pi}\int_{-\infty}^{\infty}(\alpha_1\gamma_1 A_1\mathrm{e}^{-\gamma_1 y}+\alpha_2\gamma_2 A_2\mathrm{e}^{-\gamma_2 y})\frac{\mathrm{e}^{-\mathrm{i}\omega x}}{\omega}\,\mathrm{d}\omega,\\
\frac{\tau_{xy}^*}{\mu_{12}} &= -\frac{1}{2\pi}\int_{-\infty}^{\infty}(\gamma_1 A_1\mathrm{e}^{-\gamma_1 y}+\gamma_2 A_2\mathrm{e}^{-\gamma_2 y})\mathrm{e}^{-\mathrm{i}\omega x}\,\mathrm{d}\omega-\frac{1}{2\pi}\int_{-\infty}^{\infty}(\alpha_1 A_1\mathrm{e}^{-\gamma_1 y}+\alpha_2 A_2\mathrm{e}^{-\gamma_2 y})\mathrm{e}^{-\mathrm{i}\omega x}\,\mathrm{d}\omega.
\end{aligned}\tag{19}$$

Substitution of the expression for σ_y^*, the second of Eq. (19), into the boundary condition for σ_y^*, the first of Eq. (12), yields

$$\begin{aligned}
&A_2(\omega,s) = -\beta A_1(\omega,s),\\
&\beta = \frac{c_{22}\alpha_1\gamma_1 - c_{12}\omega^2}{c_{22}\alpha_2\gamma_2 - c_{12}\omega^2} = \frac{c_{22}(c_{11}\omega^2 + s^2/c_s^2 - \gamma_1^2) - c_{12}(1+c_{12})\omega^2}{c_{22}(c_{11}\omega^2 + s^2/c_s^2 - \gamma_2^2) - c_{12}(1+c_{12})\omega^2}.
\end{aligned}\tag{20}$$

Using this result in the expression for shear stress, the third of Eq. (19), and the expression for horizontal displacement, the first of Eq. (18), we obtain

$$\begin{aligned}
\tau_{xy}^* &= -\frac{\mu_{12}}{2\pi}\int_{-\infty}^{\infty}[(\alpha_1+\gamma_1)\mathrm{e}^{-\gamma_1 y}-\beta(\alpha_2+\gamma_2)\mathrm{e}^{-\gamma_2 y}]A_1\mathrm{e}^{-\mathrm{i}\omega x}\,\mathrm{d}\omega,\\
u^* &= \frac{1}{2\pi}\int_{-\infty}^{\infty}[\mathrm{e}^{-\gamma_1 y}-\beta\mathrm{e}^{-\gamma_2 y}]A_1\mathrm{e}^{-\mathrm{i}\omega x}\,\mathrm{d}\omega.
\end{aligned}\tag{21}$$

Applying the remaining boundary conditions yields

$$\begin{aligned}
&-\frac{\mu_{12}}{2\pi}\int_{-\infty}^{\infty}[(\alpha_1+\gamma_1)-\beta(\alpha_2+\gamma_2)]A_1\mathrm{e}^{-\mathrm{i}\omega x}\,\mathrm{d}\omega = -q/s\,\delta(x+a)+\tau_+^*(x,s),\\
&\frac{1}{2\pi}\int_{-\infty}^{\infty}[1-\beta]A_1\mathrm{e}^{-\mathrm{i}\omega x}\,\mathrm{d}\omega = u_-^*(x,s).
\end{aligned}\tag{22}$$

By Fourier transform inversion, these equations become

$$-\mu_{12}[(\alpha_1+\gamma_1)-\beta(\alpha_2+\gamma_2)]A_1 = -q/s\mathrm{e}^{-\mathrm{i}\omega a}+\Sigma_+(\omega),(1-\beta)A_1 = U_-(\omega),\tag{23}$$

where

$$\Sigma_+(\omega) = \int_0^\infty \tau_+^*(x,s)\mathrm{e}^{\mathrm{i}\omega x}\,\mathrm{d}x,$$
$$U_-(\omega) = \int_{-\infty}^0 u_-^*(x,s)\mathrm{e}^{\mathrm{i}\omega x}\mathrm{d}x. \tag{24}$$

Eliminating A_1 from Eq. (23), we obtain a Wiener–Hopf equation,

$$\mu_{12}C\frac{R(\omega,s)}{\sqrt{\omega^2+s^2/c_\mathrm{s}^2}}U_-(\omega) = -q/s\mathrm{e}^{-\mathrm{i}\omega a} + \Sigma_+(\omega), \tag{25}$$

where we have introduced the function

$$R(\omega,s) = -\frac{\sqrt{\omega^2+s^2/c_\mathrm{s}^2}}{(1-\beta)C}[(\alpha_1+\gamma_1)-\beta(\alpha_2+\gamma_2)], \tag{26}$$

$$C = -\frac{1}{c_{22}(1+c_{12})N_1N_2(N_1+N_2)}\{c_{12}c_{22}N_1^2N_2^2 - c_{12}^2(1+c_{12})N_1N_2 + c_{11}[c_{22}(N_1^2+N_2^2) + c_{22}(1+c_{12})N_1N_2 + (c_{12}+c_{12}^2-c_{11}c_{22})]\}, \tag{27}$$

$$N_{1,2}^2 = \frac{1}{2c_{22}}\left\{(c_{11}c_{22}-c_{12}^2-2c_{12}) \pm [(c_{11}c_{22}-c_{12}^2-2c_{12})^2 - 4c_{11}c_{22}]^{1/2}\right\}. \tag{28}$$

After algebraic manipulation, it is found that function $R(\omega,s)$ can be written as

$$R(\omega,s) = -\frac{\sqrt{\omega^2+s^2/c_\mathrm{s}^2}}{c_{22}(1+c_{12})\gamma_1\gamma_2(\gamma_1+\gamma_2)C}\{c_{12}c_{22}\gamma_1^2\gamma_2^2 - c_{12}^2(1+c_{12})\gamma_1\gamma_2\omega^2 + (c_{11}\omega^2+s^2/c_\mathrm{s}^2)[c_{22}(\gamma_1^2+\gamma_2^2) + c_{22}(1+c_{12})\gamma_1\gamma_2 + (c_{12}+c_{12}^2-c_{11}c_{22})\omega^2 - c_{22}s^2/c_\mathrm{s}^2]\}. \tag{29}$$

From the physics of the problem, it is reasonable to assume that the functions $\tau_+^*(x,s)$ and $u_-^*(x,s)$ are exponentially bounded at infinity, which ensures the existence of their Fourier transform (24). In particular, it is shown by Noble (1958) that if $|\tau_+^*(x,s)| < M_1\mathrm{e}^{\lambda_- x}$ as $x \to +\infty$ then $\Sigma_+(\omega)$ is analytic in $\mathrm{Re}(\omega) = \lambda > \lambda_-$, and if $|u_-^*(x,s)| < M_2\mathrm{e}^{\lambda_+ x}$ as $x \to -\infty$ then $U_-(\omega)$ is analytic in $\mathrm{Re}(\omega) = \lambda < \lambda_+$.

The function $R(\omega,s)$ is analytic everywhere in the complex plane except at the branch cuts of the functions γ_i between $\omega = \pm\mathrm{i}s/c_\mathrm{s}$ and $\omega = \pm\mathrm{i}s/c_\mathrm{d}$; it is single valued in the cut ω-plane as shown in Fig. 2. It can be shown that only zeros of $R(\omega,s)$ are of the form $\pm\mathrm{i}s/c_\mathrm{R}$, where c_R is the Rayleigh wave speed. This can be seen by substituting $\omega = \mathrm{i}s/v$ in $R(\omega,s)$, letting $R(\omega,s) = 0$ and dividing by the non-zero factors, then $R(\mathrm{i}s/v,s) = 0$ reduces to

$$\sqrt{\frac{c_{22}}{c_{11}}}\left(\frac{c_{22}c_{11}-c_{12}^2}{c_{22}} - \frac{v^2}{c_\mathrm{s}^2}\right)\sqrt{1-\frac{v^2}{c_\mathrm{s}^2}} - \frac{v^2}{c_\mathrm{s}^2}\sqrt{1-\frac{v^2}{c_{11}c_\mathrm{s}^2}} = 0, \tag{30}$$

which is the Rayleigh wave function for orthotropic materials (Ting, 1996). The roots of this function are $v = \pm c_\mathrm{R}$.

4. Wiener–Hopf technique

To solve the Wiener–Hopf equation (25), we use the Wiener–Hopf technique as follows. The function $L(\omega)$ is defined and factored as

$$L(\omega) = L_+(\omega)L_-(\omega) = \mu_{12}C\frac{R(\omega,s)}{\sqrt{\omega^2 + s^2/c_s^2}}, \tag{31}$$

then the Wiener–Hopf equation becomes

$$L_-(\omega)U_-(\omega) = \frac{-q/s\mathrm{e}^{\mathrm{i}\omega a}}{L_+(\omega)} + \frac{\Sigma_+(\omega)}{L_+(\omega)}. \tag{32}$$

If the function $D(\omega)$ can be written and decomposed as

$$D(\omega) = -\frac{q/s\mathrm{e}^{-\mathrm{i}\omega a}}{L_+(\omega)} = D_+(\omega) + D_-(\omega), \tag{33}$$

then the Wiener–Hopf equation (32), is further reduced to

$$D_+(\omega) + \Sigma_+(\omega)/L_+(\omega) = L_-(\omega)U_-(\omega) - D_-(\omega) = W(\omega). \tag{34}$$

The first expression for $W(\omega)$ in Eq. (34) is analytic in the right-half plane, $\mathrm{Re}(\omega) > \lambda_-$, and the second expression is analytic in the left-half plane, $\mathrm{Re}(\omega) < \lambda_+$. If $\lambda_- > \lambda_+$, the regions of analyticity overlap and by invoking analytic continuation, it is concluded that $W(\omega)$ is analytic and single valued in the whole ω-plane shown in Fig. 2. Furthermore, invoking the extended Louisville theorem, it can be shown (Noble, 1958) that if $W(\omega)$ is bounded and entire and $W(\omega) \to 0$ as $\omega \to \infty$, then $W(\omega) = 0$. Hence, we can solve for the transform of stress ahead of the crack tip, $\Sigma_+(\omega)$, and displacement, $U_-(\omega)$, behind

$$\Sigma_+(\omega) = -D_+(\omega)L_+(\omega), \quad U_-(\omega) = \frac{D_-(\omega)}{L_-(\omega)}. \tag{35}$$

Following this outline, the first step is to factor $L(\omega)$, Eq. (31), by defining

$$F(\omega) = \frac{R(\omega,s)}{\omega^2 + s^2/c_R^2}. \tag{36}$$

Note that by making $\omega = \mathrm{i}s\varsigma$ in Eq. (36), then $F(\omega)$ is changed to a function only of ς,

$$\hat{F}(\varsigma) = \frac{R(\mathrm{i}s\varsigma, s)}{-s^2\varsigma^2 + s^2/c_R^2}. \tag{37}$$

According to Eq. (37), it is readily shown that the function $\hat{F}(\varsigma)$ is regular (i.e. analytic and single valued) in the cut ς-plane shown in Fig. 3, and $\hat{F}(\varsigma) \neq 0$ in the cut ς-plane by referring to Eq. (30). It can be shown that $\hat{F}(\varsigma) \to 1$ as $\varsigma \to \infty$ (the constant C in Eq. (27) was chosen to make this possible). The only singularities of $\hat{F}(\varsigma)$ are the branch points shared with $\gamma_i, (i = 1, 2)$, i.e. $\varsigma = \pm 1/c_s$ and $\varsigma = \pm 1/c_d$. It is well known that factorization of a function is accomplished most directly for functions which approach unity as $|\varsigma| \to \infty$ and which have neither zeros nor poles in the finite plane. Indeed, $\hat{F}(\varsigma)$ is an example of such a function. Therefore, using Cauchy's integral formula, it can be shown that (Freund, 1990)

$$\hat{F}_\pm(\varsigma) = \exp\left\{\frac{1}{2\pi\mathrm{i}}\int_{\Gamma_\pm}\frac{\log\hat{F}(\xi)}{\xi - \varsigma}\,\mathrm{d}\xi\right\}, \tag{38}$$

where Γ_- is the closed counter-clockwise contour enclosing the branch points $+1/c_d$ and $+1/c_s$, and also Γ_+ is the closed counter-clockwise contour enclosing the branch points $-1/c_d$ and $-1/c_s$.

Using the fact that $\hat{F}(\bar{\varsigma}) = \hat{F}(\varsigma)$, $H(-\eta) = -H(\eta)$, then

$$\hat{F}_\pm(\varsigma) = \exp\left\{-\frac{1}{\pi}\int_{1/c_d}^{1/c_s} H(\eta)\frac{\mathrm{d}\eta}{\eta \pm \varsigma}\right\}, \tag{39}$$

where

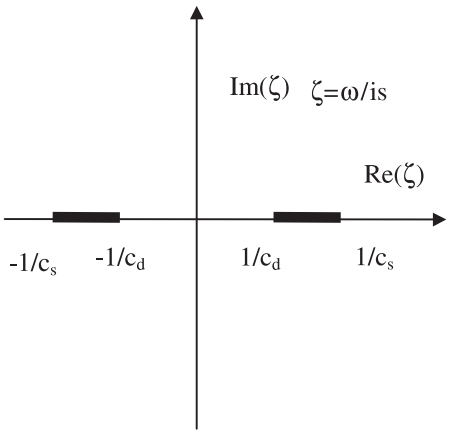

Fig. 3. Branch cuts in the ζ-plane.

$$H(\eta) = \tan^{-1}\left(\frac{\mathrm{Im}[\hat{F}(\eta)]}{\mathrm{Re}[\hat{F}(\eta)]}\right).$$

By making $\varsigma = \omega/is$ in Eq. (39), then $\hat{F}_{\pm}(\varsigma)$ is changed to $F_{\pm}(\omega)$.

Returning to the factorization of $L(\omega)$, we now have

$$L(\omega) = L_{+}(\omega)L_{-}(\omega) = \mu_{12}C\frac{F_{+}(\omega)F_{-}(\omega)(\omega + \mathrm{i}s/c_{\mathrm{R}})(\omega - \mathrm{i}s/c_{\mathrm{R}})}{\sqrt{\omega + \mathrm{i}s/c_{\mathrm{s}}}\sqrt{\omega - \mathrm{i}s/c_{\mathrm{s}}}}. \tag{40}$$

Therefore,

$$\begin{aligned} L_{-}(\omega) &= \mu_{12}C\frac{(\omega - \mathrm{i}s/c_{\mathrm{R}})}{\sqrt{\omega - \mathrm{i}s/c_{\mathrm{s}}}}F_{-}(\omega), \\ L_{+}(\omega) &= \frac{(\omega + \mathrm{i}s/c_{\mathrm{R}})}{\sqrt{\omega + \mathrm{i}s/c_{\mathrm{s}}}}F_{+}(\omega). \end{aligned} \tag{41}$$

Substituting Eq. (41) into Eq. (33), the function $D(\omega)$ can be obtained:

$$D(\omega) = \frac{-q/s\mathrm{e}^{-\mathrm{i}\omega a}}{L_{+}(\omega)} = -\frac{\sqrt{\omega + \mathrm{i}s/c_{\mathrm{s}}}}{(\omega + \mathrm{i}s/c_{\mathrm{R}})}\frac{q/s\mathrm{e}^{-\mathrm{i}\omega a}}{F_{+}(\omega)}. \tag{42}$$

Through Cauchy's integral formula, we obtain

$$D_{\pm}(\omega) = \frac{1}{2\pi\mathrm{i}}\int_{C_{\pm}}\frac{D(z)}{z - \omega}\,\mathrm{d}z = -\frac{q}{s}\left\{\frac{1}{2\pi\mathrm{i}}\int_{C_{\pm}}\frac{\sqrt{z + \mathrm{i}s/c_{\mathrm{s}}}}{(z - \omega)(z + \mathrm{i}s/c_{\mathrm{R}})}\frac{\mathrm{e}^{-\mathrm{i}za}}{F_{+}(z)}\,\mathrm{d}z\right\}, \tag{43}$$

where C_{-} is the closed counter-clockwise contour enclosing the branch points $+\mathrm{i}s/c_{\mathrm{d}}$ and $+\,\mathrm{i}s/c_{\mathrm{s}}$, and C_{+} is the closed counter-clockwise contour enclosing the branch points $-\mathrm{i}s/c_{\mathrm{d}}$ and $-\,\mathrm{i}s/c_{\mathrm{s}}$.

Thus, we can show that $W(\omega) = 0$, and using equation (35), we can readily obtain $\Sigma_{+}(\omega)$ and $U_{-}(\omega)$. We only give $\Sigma_{+}(\omega)$ here:

$$\Sigma_{+}(\omega) = -D_{+}(\omega)L_{+}(\omega) = \frac{q}{s}\frac{F_{+}(\omega)}{2\pi\mathrm{i}}\frac{(\omega + \mathrm{i}s/c_{\mathrm{R}})}{\sqrt{\omega + \mathrm{i}s/c_{\mathrm{s}}}}\int_{C_{+}}\frac{\sqrt{z + \mathrm{i}s/c_{\mathrm{s}}}}{(z - \omega)(z + \mathrm{i}s/c_{\mathrm{R}})}\frac{\mathrm{e}^{-\mathrm{i}za}}{F_{+}(z)}\,\mathrm{d}z. \tag{44}$$

5. Stress intensity factor

To find the stress intensity factor, an asymptotic expression for the shear stress near the crack tip is sought. A well-known result relating asymptotic expressions between a function and its Fourier transform (Abelian theorem's, Noble, 1958) is

$$\lim_{x\to 0_+}\sqrt{x}\tau_+^*(x,s)=\lim_{\omega\to+\infty}\mathrm{e}^{-\mathrm{i}\pi/4}\sqrt{\frac{\omega}{\pi}}\Sigma_+(\omega). \tag{45}$$

Thus, the usual definition of the stress intensity factor gives

$$\begin{aligned}&K_{\mathrm{II}}^*(s)=\lim_{x\to 0_+}\sqrt{2\pi x}\tau^*(x,s)=\lim_{\omega\to+\infty}\mathrm{e}^{-\mathrm{i}\pi/4}\sqrt{2\omega}\Sigma_+(\omega)=\lim_{\omega\to+\infty}\Phi(\omega),\\&\Phi(\omega)=\mathrm{e}^{-\mathrm{i}\pi/4}\sqrt{2\omega}\Sigma_+(\omega).\end{aligned} \tag{46}$$

As $\omega\to+\infty$, $\Phi(\omega)$ becomes

$$\Phi(\omega)=-\frac{\sqrt{2}q}{s}\frac{\mathrm{e}^{-\mathrm{i}/4}}{2\pi\mathrm{i}}\int_{C_+}\frac{\sqrt{z+\mathrm{i}s/c_\mathrm{s}}}{(z+\mathrm{i}s/c_\mathrm{R})}\frac{\mathrm{e}^{-\mathrm{i}za}}{F_+(z)}\,\mathrm{d}z. \tag{47}$$

By making $z=\mathrm{i}s\varsigma$, Eq. (47) becomes

$$\Phi(\omega)=-\frac{\sqrt{2}q}{s^{1/2}}\frac{1}{2\pi\mathrm{i}}\int_{\Gamma_+}\frac{\sqrt{\varsigma+1/c_\mathrm{s}}}{(\varsigma+1/c_\mathrm{R})}\frac{\mathrm{e}^{s\varsigma a}}{\hat{F}_+(\varsigma)}\,\mathrm{d}\varsigma\quad\text{as }\omega\to+\infty. \tag{48}$$

Thus,

$$K_{\mathrm{II}}^*(s)=-\sqrt{2}q\left\{\frac{1}{2\pi\mathrm{i}}\int_{\Gamma_+}g(\varsigma)\,\mathrm{d}\varsigma\right\}, \tag{49}$$

where

$$g(\varsigma)=\frac{\sqrt{\varsigma+1/c_\mathrm{s}}}{(\varsigma+1/c_\mathrm{R})\hat{F}_+(\varsigma)}\frac{\mathrm{e}^{s\varsigma a}}{s^{1/2}}.$$

Note that $g(\bar{\varsigma})=\overline{g(\varsigma)}$, and $g(\varsigma)\to 0$ *as* $|\varsigma|\to\infty$ in the left-half plane. Also, note that $\hat{F}_+(-\varsigma)=\hat{F}_-(\varsigma)$. Consequently, Eq. (49) can be written as the real integral

$$\begin{aligned}K_{\mathrm{II}}^*(s)&=-\sqrt{2}q\left\{\frac{1}{\pi}\int_{-1/c_\mathrm{d}}^{-\eta^*}\mathrm{Im}[g(\eta)]\,\mathrm{d}\eta\right\}\\&=\frac{\sqrt{2}q}{\pi}\int_{1/c_\mathrm{d}}^{\eta^*}\mathrm{Im}\left(\frac{\sqrt{1/c_\mathrm{s}-\eta}}{(1/c_\mathrm{R}-\eta)\hat{F}_-(\eta)}\frac{\mathrm{e}^{-s\eta a}}{s^{1/2}}\right)\mathrm{d}\eta,\end{aligned} \tag{50}$$

where η^* is a positive real number.

Applying the inverse Laplace transform to $K_{\mathrm{II}}^*(s)$, using the convolution formula and letting $\eta^* a=t$, the stress intensity factor $K_{\mathrm{II}}(t)$ can be written as follows:

$$K_{\mathrm{II}}(t)=-q\sqrt{2/\pi\mathrm{a}}\left\{-\frac{1}{\pi}\int_{1/c_\mathrm{d}}^{t/a}\mathrm{Im}\left(\frac{\sqrt{1/c_\mathrm{s}-\eta}}{(1/c_\mathrm{R}-\eta)\sqrt{t/a-\eta}\hat{F}_-(\eta)}\right)\mathrm{d}\eta\right\}. \tag{51}$$

The integrand of Eq. (51) has a first-order singularity at $\varsigma=1/c_\mathrm{R}$ and branch points at $\varsigma=1/c_\mathrm{d}$, $\varsigma=1/c_\mathrm{s}$ and $\varsigma=\varsigma_0=t/a$, which is shown in Fig. 4. Here, pay attention to those points at

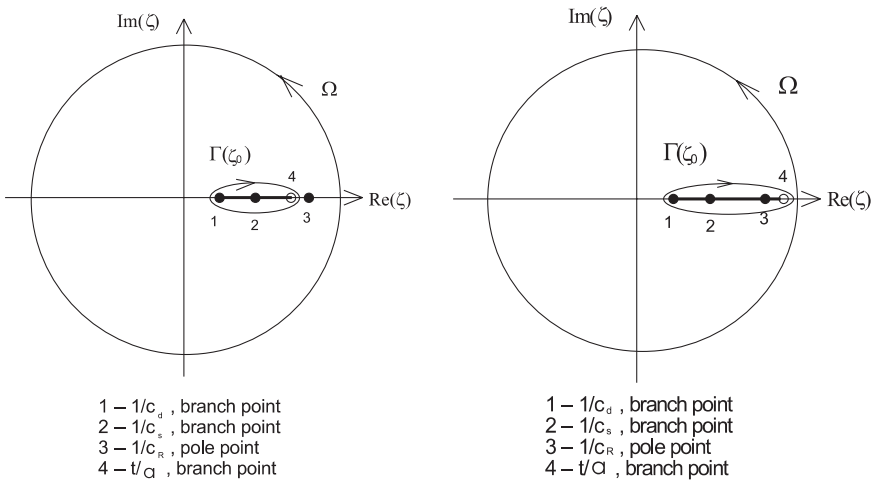

Fig. 4. Branch cuts in the ζ-plane and integral path.

$\varsigma = 1/c_{\mathrm{d}}, \varsigma = 1/c_{\mathrm{s}}, \varsigma = \varsigma_0 = t/a$ and $\varsigma = 1/c_{\mathrm{R}}$, which are critical of the integrand of Eq. (51) as shown in the Fig. 4.

For $t/a < 1/c_{\mathrm{d}}$, no waves generated by the applied loads have arrived at the crack tip, hence, the stress intensity factor $K_{\mathrm{II}}(t)$ is identically zero.

For $1/c_{\mathrm{d}} < t/a < 1/c_{\mathrm{s}}$, a direct evaluation procedure for the stress intensity factor $K_{\mathrm{II}}(t)$ cannot be applied to the integral. It has to be obtained by numerical evaluation.

For $t/a > 1/c_{\mathrm{s}}$, the integrand of Eq. (51) is analytic in the entire ζ-plane cut along $1/c_{\mathrm{d}} < \mathrm{Re}(\zeta) < t/a$, $\mathrm{Im}(\zeta) = 0$, except for the pole point at $\varsigma = 1/c_{\mathrm{R}}$. In this case, the path of integration can be closed around the right side of the branch cut shown in Fig. 4. The integral (51) takes the form

$$K_{\mathrm{II}}(t) = -\frac{q\sqrt{2}}{2\pi \mathrm{i}\sqrt{\pi a}} \oint_{\Gamma(\varsigma_0)} \frac{\sqrt{1/c_{\mathrm{s}} - \varsigma}}{(1/c_{\mathrm{R}} - \varsigma)} \frac{1}{\sqrt{t/a - \varsigma}} \frac{1}{\hat{F}_-(\varsigma)} \,\mathrm{d}\varsigma, \tag{52}$$

where $\Gamma(\varsigma_0)$ denotes a closed counter-clockwise contour embracing the branch cut of the integrand. Cauchy's integral formula can now be applied to show that the value of the integral in Eq. (51) is equal to the value of the integral taken along a closed counter-clockwise circular path of indefinitely large radius, (Ω), in ζ-plane shown in Fig. 4. Therefore,

$$\frac{K_{\mathrm{II}}(t)}{-q\sqrt{2}/\pi a} = 1 - \begin{cases} \frac{(1/c_{\mathrm{R}} - 1/c_{\mathrm{s}})^{1/2}}{(1/c_{\mathrm{R}} - t/a)^{1/2} \hat{F}_-(1/c_{\mathrm{R}})} & \text{if } 1/c_{\mathrm{s}} < t/a < 1/c_{\mathrm{R}}, \\ 0 & \text{if } t/a > 1/c_{\mathrm{R}}. \end{cases} \tag{53}$$

The first term on the right-hand side of Eq. (53) is the contribution from the closed contour of the large radius and the second term is the residue contribution. In addition, the first term in Eq. (53) is the corresponding static solution for a semi-infinite crack under shear concentrated forces applied on its faces, $K_{\mathrm{II}}(t) = -q\sqrt{2/\pi a}$.

6. Results and discussion

Using Eqs. (52) and (53), the stress intensity factor $K_{\mathrm{II}}(t)$ can be calculated. The computed results are shown in Figs. 5–8 for several materials, and the mechanical properties (Schwartz, 1997) used for the

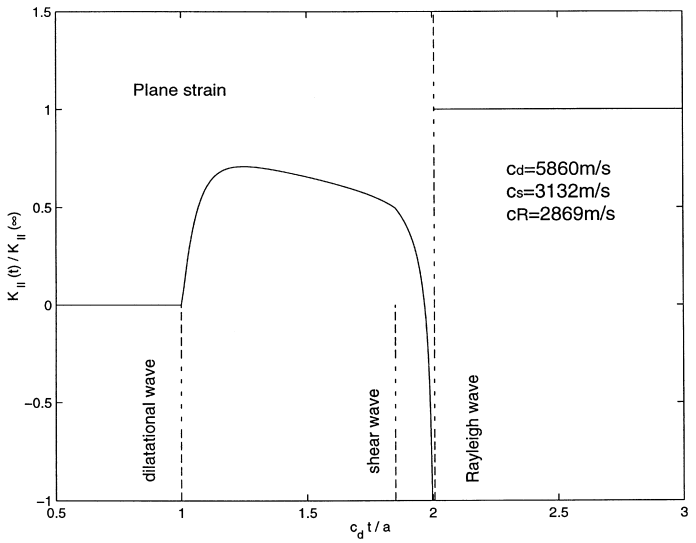

Fig. 5. Stress intensity factor history in an isotropic material under concentrated shear loads.

analysis are given in Table 1. The following tips should be taken into account when performing the numerical evaluation of the integral in Eq. (51).

(1) Theoretically, $R(\omega,s)$ in Eq. (26) can include either the factor $\sqrt{\omega^2+s^2/c_{\mathrm{d}}^2}$ or $\sqrt{\omega^2+s^2/c_{\mathrm{s}}^2}$, and we should have $\hat{F}(\varsigma)=1$ as $\varsigma\to\infty$. However, experience shows that if the factor $\sqrt{\omega^2+s^2/c_{\mathrm{d}}^2}$ is selected in $R(\omega,s)$, it is difficult to numerically make $\hat{F}(\varsigma)=\hat{F}_+(\varsigma)\hat{F}_-(\varsigma)$ at points in the regions close to $[1/c_{\mathrm{d}},1/c_{\mathrm{s}}]$ and $[-1/c_{\mathrm{s}},-1/c_{\mathrm{d}}]$, where $\hat{F}(\varsigma)$, $\hat{F}_-(\varsigma)$ and $\hat{F}_+(\varsigma)$ are, respectively, calculated using Eqs. (37) and (38). This is true even though $\hat{F}(\varsigma)=1$ and $\hat{F}(\varsigma)=\hat{F}_+(\varsigma)\hat{F}_-(\varsigma)$ at points very far from $[1/c_{\mathrm{d}},1/c_{\mathrm{s}}]$ and $[-1/c_{\mathrm{s}},-1/c_{\mathrm{d}}]$. For the problem with concentrated normal loads (Rubio-Gonzalez and Mason 1998c), the factor $\sqrt{\omega^2+s^2/c_{\mathrm{d}}^2}$ should be selected in $R(\omega,s)$, while the factor $\sqrt{\omega^2+s^2/c_{\mathrm{s}}^2}$ should be selected in $R(\omega,s)$ for the problem in this paper; otherwise, there may be large errors in the calculations.

(2) It is best to adopt the formula $\hat{F}_-(\varsigma)=\hat{F}(\varsigma)/\hat{F}_+(\varsigma)$ to indirectly calculate the values of $\hat{F}_-(\varsigma)$ along $[1/c_{\mathrm{d}},1/c_{\mathrm{s}}]$ because $\hat{F}_-(\varsigma)$ is not analytic along $[1/c_{\mathrm{d}},1/c_{\mathrm{s}}]$. At $\varsigma=1/c_{\mathrm{R}}$, the value of $\hat{F}_-(1/c_{\mathrm{R}})$ can be directly obtained by using Eq. (39).

The numerical results presented correspond to isotropic and orthotropic materials. Properties of transversely isotropic materials with fibers parallel and perpendicular to the x-axis are considered in the orthotropic case.

For isotropic materials, as mentioned in Rubio-Gonzalez and Mason (1998c), note that the mechanical parameters make $\gamma_1=\gamma_2$, and further lead to $\beta=1$ and $R(\omega,s)$ not defined. Consequently, in order to obtain the results for the isotropic case from the orthotropic formulation, we let $E_1=E$, $E_2=(1-\varepsilon)E$, $v_{12}=v_{23}=v$ and $\mu_{12}=E_2/2(1+v)$, where E and v correspond to the isotropic properties and ε is a small quantity with $\varepsilon\ll 1$.

Fig. 5 shows $K_{\mathrm{II}}(t)$ for an isotropic material in the plane-strain case. The normalization factor is the long time limit $K_{\mathrm{II}}(\infty)=-q\sqrt{2/\pi a}$ and the normalized time is $c_{\mathrm{d}}t/a$. The behavior illustrated in Fig. 5 is as expected from the surface displacements in the calculated solution of Lamb's problem, where a concentrated shear load is applied on a half space (Chao, 1960). Horizontal displacements on the surface, generated by the point load, arrive at the crack tip with the arrival of the dilatational wave causing a rapid increase in the stress intensity factor. In addition, the results in Fig. 5 are very similar to that of the problem in Rubio-Gonzalez and Mason (1998b), before the arrival of the second dilatational wave, shear wave and

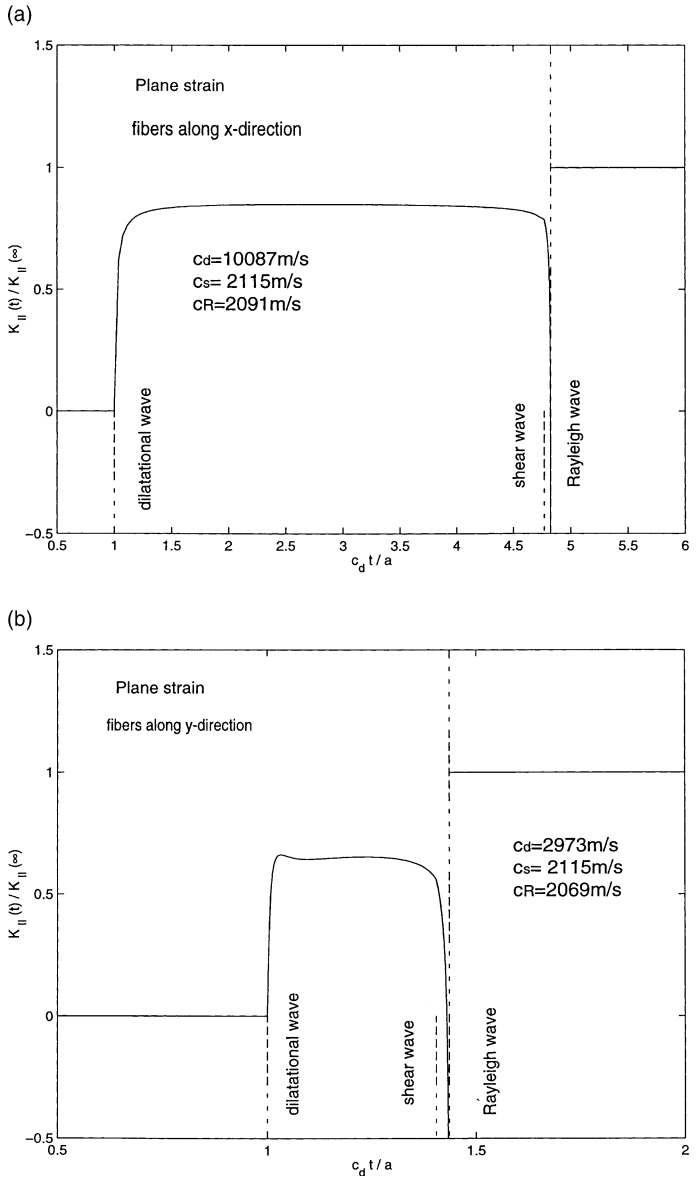

Fig. 6. Stress intensity factor history in graphite epoxy under concentrated shear loads.

Rayleigh wave, where a finite crack in infinite orthotropic body is impacted by two pairs of concentrated shear loads. After the arrival of the dilatational wave, a rapid increase in $K_{\mathrm{II}}(t)$ is observed, and then the stress intensity factor gradually decreases until the shear wave front arrives at $t = a/c_{\mathrm{s}}$. Thereafter, the stress intensity factor decreases rapidly to a negative square root singularity at $t = a/c_{\mathrm{R}}$, which is the instant of the arrival of the Rayleigh wave traveling along the crack faces from the point of application of load. For time $t > a/c_{\mathrm{R}}$, the stress intensity factor takes on the constant value $-q\sqrt{2/\pi a}$, which is the equilibrium stress intensity factor for the specified loading. Obviously, the dilatational wave has an important effect on $K_{\mathrm{II}}(t)$ under applied concentrated impact shear loads, unlike applied concentrated impact normal loads

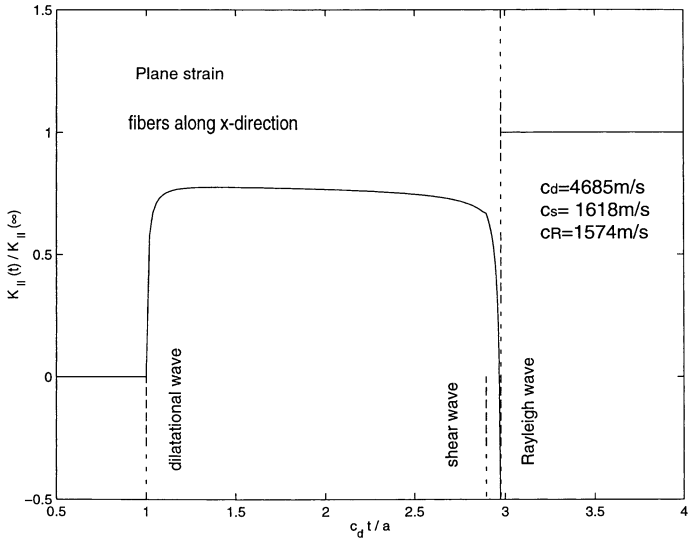

Fig. 7. Stress intensity factor history in E-glass epoxy under concentrated shear loads.

where the dilatational wave has a minimum effect on $K_I(t)$ (Rubio-Gonzalez and Mason, 1998a,c). The stress intensity factor for an isotropic material in the plane-stress case is identical to the plane-strain case except for differences in the dilatational wave speed.

Fig. 6(a) and (b) shows the stress intensity factor history for a graphite–epoxy composite in the plane-strain state with fibers parallel to the x-axis and y-axis, respectively. Both figures are similar to the results for the isotropic material shown in Fig. 5, except that there is a more uniform plateau from $t = a/c_d$ to $t = a/c_s$ and a steeper drop at $t = a/c_R$. In Fig. 6(b), the plateau is lower than in Fig. 6(a) and the duration of the plateau is longer due to the dramatic difference in c_d for these two cases. The Rayleigh wave speeds are approximately the same; the shear wave speeds are exactly the same.

As expected, the behavior illustrated in Fig. 6(b) is the same as that for the corresponding case of Rubio-Gonzalez and Mason (1998b) before the second set of waves arrives crack tip. The behavior illustrated in Fig. 6(a) cannot be directly compared with that of the corresponding case of Rubio-Gonzalez and Mason (1998b) because in that work the second dilatational wave arrived at the crack tip before the arrival of the first shear wave and Rayleigh wave leading to very different loading conditions. To the knowledge of the authors, this is the first presentation of results for this case that are not disturbed by reflected or secondary waves.

Figs. 7 and 8(a) show the stress intensity factor history for the E-glass epoxy and boron epoxy composites in the plane strain state, respectively. In both the cases, the fibers are oriented along the x-axis. Figs. 7 and 8(a) are very similar to Fig. 6(a). Fig. 8(b) shows the singularity at $t = a/c_R$ more clearly. The singularity can be quite difficult to capture using the method of Rubio-Gonzalez and Mason (1998b) because the shear and Rayleigh wave speeds are nearly equal. Here, Eq. (53) gives $K_{II}(t)$ explicitly.

7. Conclusions

(1) For impact concentrated shear loads on a semi-infinite crack in an orthotropic material, the arrival of the dilatational wave at the crack tip makes an important contribution to the dynamic stress intensity factor $K_{II}(t)$, unlike in mode I loading, where dilatational wave had a minimum effect on $K_I(t)$.

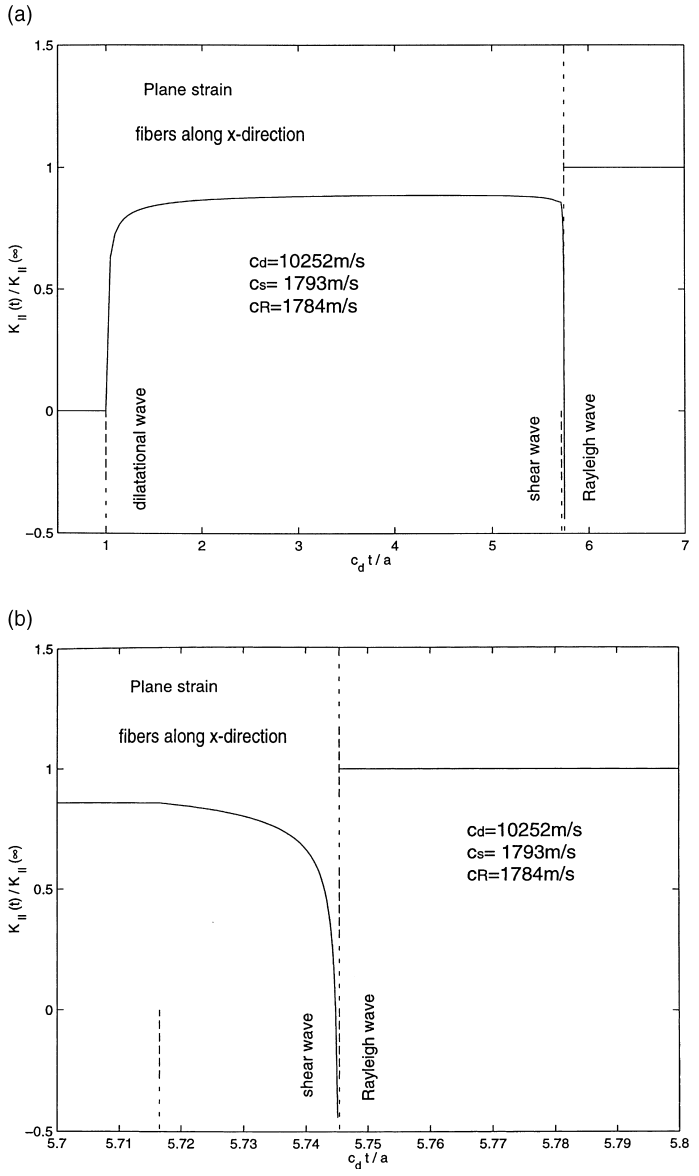

Fig. 8. Stress intensity factor history in boron epoxy under concentrated shear loads.

(2) The long time value, $K_{\mathrm{II}}(\infty) = -q\sqrt{2/\pi a}$, is independent of the mechanical properties of the orthotropic material, however the curve shape and magnitude of $K_{\mathrm{II}}(t)$ from $t = a/c_{\mathrm{d}}$ to $t = a/c_{\mathrm{R}}$ is very dependent on the mechanical properties of materials.

(3) From the results given here for an isotropic material and orthotropic materials, we can conclude that the normalized $K_{\mathrm{II}}(t)$ from $t = a/c_{\mathrm{d}}$ to $t = a/c_{\mathrm{R}}$ is less than 1 except at a singularity at $t = a/c_{\mathrm{R}}$. In addition, under similar conditions, when fibers are parallel to the crack direction $K_{\mathrm{II}}(t)$ is generally greater than when the fibers are perpendicular to the crack direction.

Table 1
Mechanical properties used for the analysis

	Isotropic material	Graphite epoxy	E-glass epoxy	Boron epoxy
E_1(Gpa)	200	156.75	45	207
E_2(Gpa)	200	10.41	12	19
ν_{12}	0.3	0.31	0.19	0.21
ν_{23}	0.3	0.49	0.19	0.21
μ_{12}(Gpa)	76.92	7.07	5.5	6.4
ρ(Kg/m^3)	7840	1580	2100	1990

(4) Finally, the method outlined here can easily be extended to solve the problem of a semi-infinite crack under more general impact shear loads on the faces of a semi-infinite crack. Alternatively, the solution presented here can be used as a Green's function to solve more general problems. Both methods should yield the same results.

Acknowledgements

Support of this work by the Office of Naval Research Young Investigator Program under grant N00014-96-1-0774 supervised by Dr. Y. Rajapakse and the Mexican Government through CONACYT (Consejo Nacional de Ciencia y Tecnologia) is gratefully acknowledged.

References

Chao, C.C., 1960. Dynamic response of an elastic half-space to tangential surface loadings. ASME J. Appl. Mech. 27, 559–567.
Freund, L.B., 1974. The stress intensity factor due to normal impact loading on the faces of a crack. Int. J. Engng. Sci. 12, 179–189.
Freund, L.B., 1990. Dynamic Fracture Mechanics. Cambridge University Press, New York.
Kassir, M.K., Bandyopadhyay, K.K., 1983. Impact response of a cracked orthotropic medium. ASME J. Appl. Mech. 50, 630–636.
Kuo, M.K., Chen, T.Y., 1992. The Wiener–Hopf technique in elastodynamic crack problems with characteristic lengths in loading. Engng. Fract. Mech. 42, 805–813.
Nayfeh, A.H., 1995. Wave propagation in anisotropic media with applications to composites. North-Holland, Amsterdam.
Noble B, 1958. Methods based on the Wiener-Hopf Technique. Pergamon, New York.
Poruchikov, V.B., 1993. Methods of the Classical Theory of Elastodynamics. Springer, New York.
Rubio-Gonzalez, C., Mason, J.J., 1998a. Fundamental solutions for the stress intensity factor evolution in finite cracks in orthotropic materials. Int. J. Fract., to appear.
Rubio-Gonzalez, C., Mason, J.J., 1998b. Response of finite cracks in orthotropic materials due to concentrated impact shear loads. J. Appl. Mech. 66, 485–491.
Rubio-Gonzalez, C., Mason, J.J., 1998c. Dynamic stress intensity factor for a semi-infinite crack in orthotropic materials due to concentrated normal impact loads. J. Comp. Mater., to appear.
Rubio-Gonzalez, C., Mason, J.J., 1998d. Closed form solutions for dynamic stress intensity factors at the tip of uniformly loaded semi-infinite cracks in orthotropic materials. J. Mech. Phys. Solids. 48, 899–925.
Schwartz, M.M., 1997. Properties, nondestructive testing and repair. In: Goodwin, B.M. (Ed.), Composite Material, vol. 1. Prentice-Hall, NJ.
Sneddon, I.N., 1946. The distribution of stress in the neighborhood of a crack in an elastic solid. Proc. Roy. Soc. London A 187, 229–260.
Sneddon, I.N., 1952. The stress produced by a pulse of pressure moving along the surface of a semi-infinite solid. Rend. Cir. Mat. Palermo 1, 57–62.
Ting, T.C.T., 1996. Anisotropic elasticity. Oxford University Press, New York.
Willis, J.R., 1973. Self-similar Problems in Elastodynamics. Philos. Trans. Roy. Soc. London Series A 274, 435–491.